ESF-SILMI-Report on the short visit grant No 5003

Numerical analysis of fast electron transport in planar compressed targets

Xavier Vaisseau[1], João Santos[1], Arnaud Debayle[2] and José Javier Honrubia[2]

[1]CELIA, Université Bordeaux 1/CNRS/CEA, Talence, France
[2]ETSI Aeronauticos, Universidad Politécnica, Madrid, Spain

1 Purpose of the visit

The goal of the visit of the group of J.J Honrubia and Arnaud Debayle at the ETSI Aeronautica (Univesidad Politécnica de Madrid) was to initiate the numerical analysis of a fast electron transport experiment performed in July 2011 on the TITAN laser facility (LLNL, USA). This experiment is to been seen in the fast ignition scheme (FI) for energy production in the the inertial confinement fusion context (ICF)[1]. The aim was mostly related to the fast electron transport in dense plasmas.

The settlement of the FI scheme needs indeed a deep understanding of the suprathermal electrons transport in a representative panel of ICF plasmas. This phenomenon was particularly studied in solid and cold targets which are far from extreme density and temperature conditions reached in ICF targets. In particular, the electrical conductivity and the collective stopping power consequently differs dramatically. This experiment is clearly adapted to characterize the stopping power and the divergence of the fast electron beam due to both collisional and collective effects, but it focuses on the latter one. We finally highlight the fact that this experiment follows the framework of a previous campaign which took place on the LULI2000 facility (LULI, Ecole Polytechnique, France) but with higher laser intensity conditions[2].

2 Experimental work

We studied the suprathermal electron transport in a warm ($1 - 10$ eV) and dense ($\sim$ 6 g.cm^{-3}) aluminum plasma. A counter propagative compressive planar shock was generated by a long laser pulse LP ($\lambda_0 = 0.53$ μm, $\tau_0 = 5$ ns, $E_{LP} \sim 160$ J, $I_{LP} \sim 1.4.10^{14}$W.cm^{-2}) on the rear side of solid multilayer targets in order to reach about twice the solid density in the aluminum layer. A sketch of the targets structure is given in fig.1.

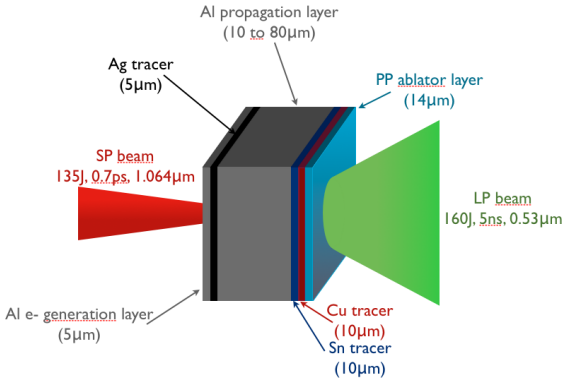

Figure 1: Target structure. The central alunimun propagation layer is surrounded by an Ag fast electron source tracer at the front side and by a Sn and Cu tracers at the rear side. The two latter ones are tracers of fast electrons which crossed the target.

The electron beam was generated by an intense laser pulse SP ($\lambda_0 = 1.064$ μm, $\tau_0 = 0.7$ ps, $E_{SP} \sim 135$ J, $I_{SP} \sim 6.10^{20}$W.cm^{-2}) before the shock breakout at the front side of the target. The planar compression ensured a wide transversal homogeneity along the electron propagation axis. A numerical study performed before the experiment with the radiative-hydrodynamic CHIC[3,4] code was necessary in order to adjust delays between the two laser beams. Two cases were indeed considered during the experiment. The solid case corresponds to a propagation of the electron beam in a solid and cold aluminum layer. The LP beam was though always fired in order to create at the rear side of the target a get lost layer in the coronal plasma which inhibited the electron recirculation. The second case is the compressed case : the SP beam was

fired when the aluminum propagation layer was compressed and heated by the LP laser shock in order to study the propagation of the fast electron beam in a dense plasma. In both solid and compressed cases, the SP amplified spontaneous emission (ASE) was taken into account by the CHIC simulations. Fig. 2a) and b) show the density and the temperature of a 20 μm propagation layer target for uncompressed and compressed targets.

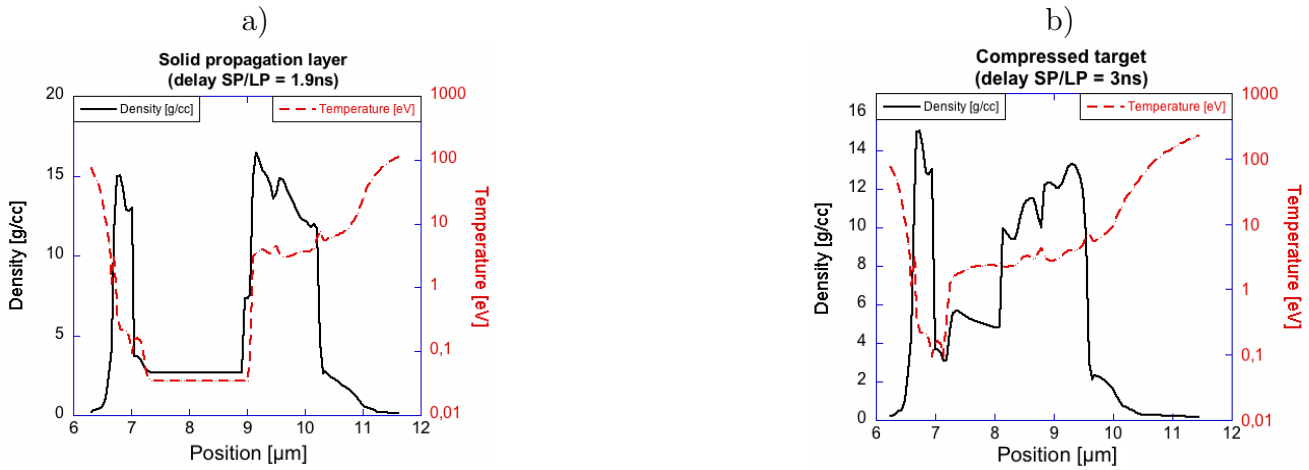

Figure 2: Density (full black curves) and temperature (red dashed curves) profiles of 20 μm propagation layer targets for a) uncompressed cases and b) compressed cases.

In the first case, the Sn and Cu rear tracers are compressed and heated while the aluminum propagation central layer is kept cold and at solid density. In the latter case, the propagation layer is almost entirely compressed and the fast electron beam see a density increased by a factor of two, except in the very first micrometers. Streaked-Optical-Pyrometry measurements were initially planned in order to benchmark the simulations. However, due to experimental issues, this diagnostic didn't work, and the SP/LP delay relied on the use of scaling laws. CHIC simulations were performed afterward in order to get hydrodynamics profiles closer to the actual laser conditions. It was also checked that the LP induced shock did not breakout before the fast electron injection.

3 Numerical work

Fast electron transport simulations were performed using the 2D axisymetric hybrid code developed by Javier Honrubia[5]. The initial parameters were the temperature and density profiles calculated by the CHIC code. The fast electron source parameters were inferred from previous simulation works at similar SP intensities. PIC simulation made by the PICLS code[6] are still in progress in order to compute a more realistic estimation of the source with the experimental laser parameters. The chosen source is described as follows :

- The energy distribution is not a simple Maxwellian function, it is described by a power law function at low energies. If E stands for an electron energy, the distribution function writes

$$f(E) = \underbrace{\exp\left(-\frac{E}{T_b}\right)}_{\text{Low energy spectrum}} + \left(\underbrace{\exp\left(\frac{T_c}{E}\right)}_{\text{Low energy cut}} \cdot \left(\frac{\gamma_0 - 1}{E}\right)^a \cdot \underbrace{\exp\left(-\frac{E}{T_{sh}}\right)}_{\text{High energy cut}} \right) \quad (1)$$

with γ_0, a, T_b, T_s, T_{sh} fit parameters given by a numerical adjustment of the PIC electron source results. The mean energy of the fast electron beam was adjusted by tuning these parameters. An example of source spectrum is given in fig 3.

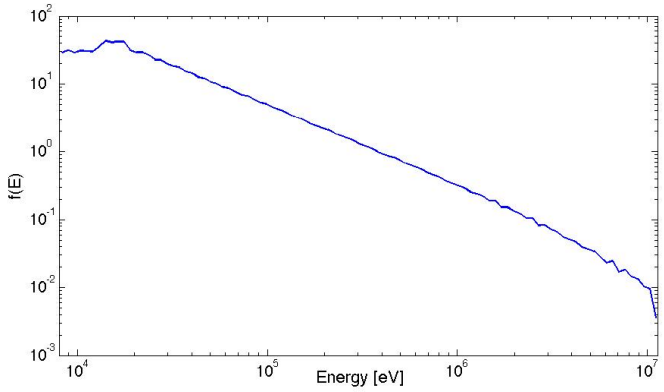

Figure 3: Exemple of the electron source energy distribution function for a mean energy close to 750 keV. The parameters are $T_b = 2000$, $T_c = 0$, $T_{sh} = 1.2.10^7$, $a = 1.15$, $\gamma_0 = 1.1$.

- The angular distribution[7] is given by

$$f(\theta) = \exp\left[-\frac{(\theta - \theta_r)^2}{(\Delta\theta_0)^2}\right] \tag{2}$$

with $\theta_r = \arctan\left(\frac{r}{r_b}\right) = 30°$ the mean radial angle, r_b the electron injection radius and $\Delta\theta_0 = 55°$ the dispersion angle.

During this visit, we only focused on the analysis of the solid cases. In order to try to reproduce the Ag-Kα, Sn-Kα and Cu-Kα yields shown in fig.4, the effect of several input parameters was studied such as the electron beam mean energy, the laser-hot electrons conversion efficiency C_{eff}, the fast electron injection radius f_{rad} and the energy spectrum tendency. Their effects are described as follows.

- A comparison between a mean energy close to 1 MeV, 750 keV and 500 keV shows that the absolute Kα yields are better reproduced for the first one. The laser-electrons conversion efficiency was set at 40% while the electron injection radius was set at 20 μm. Only the power law parameter a was changed in order to tune the electron mean energy. The Ag-Kα yield is quite close from the experimental data. However, the Sn-Kα and Cu-Kα are not reproduced. If one plot the evolution of the Sn-Kα/Ag-Kα ratio as a function of the target areal density, which is related to the fraction of fast electron with an energy > 75 keV which crossed the propagation layer, one see that the yield ratio and the trend are not reproduced : due to the rise of collisions, the simulated ratio decreases faster than the experimental ratio when increasing the propagation layer thickness. This comparison is shown in fig.4.

- The comparison between two laser-electrons conversion efficiencies, $C_{eff} = 20\%$ and $C_{eff} = 40\%$, shows that all the absolute yields are better reproduced for the first one. The electron mean energy was set at 750 keV and the injection radius was kept at 20 μm. When switching from $C_{eff} = 20\%$ to $C_{eff} = 40\%$, both collisional and resistive losses increase by a factor 2.

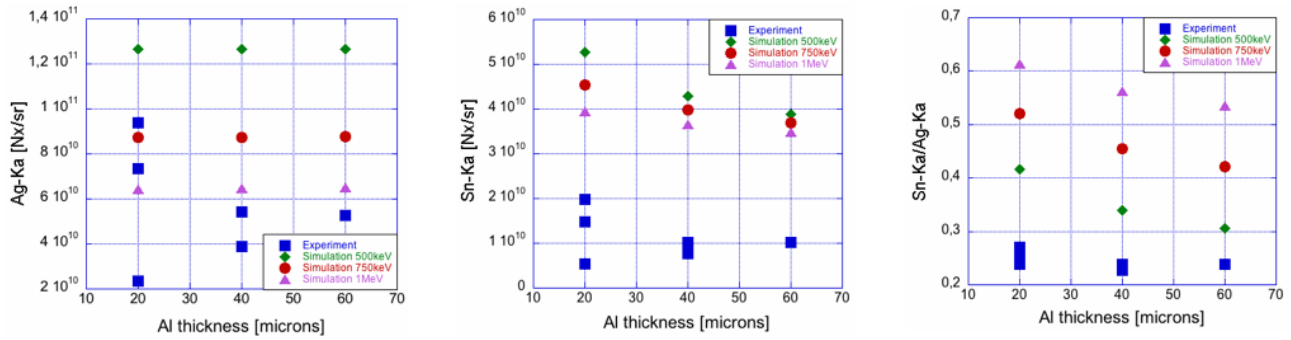

Figure 4: Ag, Sn tracers K_α absolute fluorescence yields and Sn-K_α/Ag-K_α ratio as a function of the aluminum propagation layer thickness. Symbols stand as follows : blue squares : experimental results; green lozenges : simulations at 500 keV; red circles : simulations at 750 keV; purple triangles : simulations at 1 MeV.

- The comparison between two fast electron injection radius, $f_{rad} = 20\ \mu$m and $f_{rad} = 40\ \mu$m was made. The conversion efficiency was set at 40%. The electron mean energy was first kept at 750 keV, and then moved to 1 MeV. It is observed that the absolute yields are better reproduced for $f_{rad} = 20\ \mu$m and for a mean energy close to 1 MeV. The slope of the Sn-Kα/Ag-Kα ratio is also closer to the experimental result in this latter case. Resistive losses are also more important for $f_{rad} = 20\ \mu$m.

- Finally, two PIC sources were tested. The first one is shown in fig 3. The second one is also described by eq.1 but with different parameters : $T_b = 200.10^3$, $T_c = 0$, $T_{sh} = 1.210^7$, $\gamma_0 = 1.1$, $a = 1.02$. The general trend doesn't change but the power law decreasing part is smoother in this latter case. It is observed that the Sn-K_α and Cu-K_α yields are quite similar, but the Ag-K_α yield is better reproduced for the second PIC source. The Sn-K_α/ Ag-K_α ratio is really sensitive to the fast electron energy spectrum shape.

  At the end of this visit, we couldn't reproduce the absolute Sn-K_α yield and the Sn-K_α/Ag-K_α ratio at the same time. New simulations will be lunched in the next weeks in order to better reproduce the experimental data. Then, as soon as PIC calculations are finished, the electron source distribution function will be adjusted to a more realistic one. When the simulations will be in agreement with the data points, the electron energy losses will be analyzed in order to understand the loss mechanisms. Finally, the compressed case will also be simulated and the compressed targets data will be interpreted.

4 Conclusion

This visit was mainly dedicated to understand the functioning of the hybrid numerical code. Several simulations were performed varying different parameters such as the fast electrons mean energy, the laser-electron conversion efficiency, the electron injection radius, and finally the PIC source energy spectrum aspect. Despite the variety of all these conditions, it was impossible to reproduce at the same time the Sn-K_α yield and the Sn-K_α/Ag-K_α ratio which is related to the fraction of electrons with an energy > 75 keV which crossed the target. New simulations will be launched in the next weeks with a more realistic computed PIC source, and different effects which will be taken into account. An experiment will be carried on in June 2012 on the TITAN laser facility. A part of it will be dedicated to shoot on the same target described in fig.1 in order to get extra data points. The collaboration with the UPM group for the interpretation work will certainly continue. Finally, we note that the experimental data obtained during the

TITAN campaign are quite different from the LULI2000 campaign with an SP intensity close to 10^{19}W.cm^{-2}. In particular, the Sn-K$_\alpha$/Ag-K$_\alpha$ ratio differs much more when comparing solid and compressed cases in the TITAN campaign.

5 Projected Publications

Both experimental work and simulations will be presented in several international conferences during the next year. At least one publication will also be submitted to a scientific journal.

[1]Max Tabak *et al.*, Phys. Plasmas **1**, 1626 (1994).
[2]B. Vauzour, PhD thesis (2012).
[3]P.H. Maire *et al.*, SIAM J. Sci. Comput. **29**(4), 1781 (2007).
[4]P.H. Maire and J. Breil, Int. J. Numer. Methods Fluids **56**, 1161 (2008).
[5]J. J. Honrubia *et al.*, Phys. Plasmas **12**, 052798 (2005).
[6]Y. Sentoku and A. J. Kemp, J. Comput. Phys. **227**, 6846 (2008).
[7]A. Debayle *et al.*, Phys. Rev. E **82**, 036405 (2010).